Mesoscale simulation of clay aggregate formation and mechanical properties

Mesoscale simulation of clay aggregate formation and mechanical properties

Davoud Ebrahimi†, Roland J.-M. Pellenq†§‡, Andrew J. Whittle†

†Department of Civil and Environmental Engineering Massachusetts Institute of Technology, Cambridge, MA 02139, USA and

§Centre Interdisciplinaire de Nanosciences de Marseille Aix-Marseille Universit´e, CNRS, Campus de Luminy, 13288 Marseille Cedex 09, France and

‡ < MSE >2, UMI 3466 CNRS-MIT, Cambridge, MA 02139, USA

Abstract: This paper proposes a novel methodology for understanding the meso-scale aggregation of clay platelets in water. We use Molecular Dynamics (MD) simulations using the CLAYFF force fields to represent the interactions between two layers of Wyoming montmorillonite (Na-smectite) in bulk water. The analyses are used to establish the potential of mean force at different spacings between the layers for edge-to-edge and face-to-face interactions. This is accomplished by finding the change in free energy as a function of the separation distance between the platelets using thermodynamic perturbation theory with a simple overlap sampling method. These nanoscale results are then used to calibrate the Gay-Berne (GB) potential that represents each platelet as a single-site ellipsoidal body. A coarse-graining upscaling approach then uses the GB potentials and molecular dynamics to represent the meso-scale aggregation of clay platelets (at submicron length scale). Results from meso-scale simulations obtain the equilibrium/jamming configurations for mono-disperse clay platelets. The results show aggregation for a range of clay platelets dimensions and pressures with mean stack size ranging from 3-8 platelets. The particle assemblies become more ordered and exhibit more pronounced elastic anisotropy at higher confining pressures. The results are in good agreement with previously measured nano-indentation moduli over a wide range of clay packing densities.

1. Introduction

The behavior of soil is highly affected by its clay content e.g., swelling capacity of the micropore volume decreases as clay content increases [1] but due to the small size of clay particles and the molecular scale of interaction, the behavior of clay is not yet fully understood [2]. Soil aggregation is primarily due to clay content of the soil [3]. Aggregation or dispersion of clay particles can cause changes in the microstructure and mechanical properties of the clay. The classical DLVO theory [4, 5] which is based on electrostatic and van der Waals forces fails to explain short range repulsion between clay layers. This could be due to inability of DLVO theory

in predicting structured layers of water molecules which has been reported in experiments [6, 7] and simulations [8]. As a result, DLVO theory is not able to describe the stability of the clay-water system at short range distance (where clay aggregates are formed). Molecular dynamics (MD) is an alternative computational technique to model and explain underlying mechanisms of formation of clay aggregates as it works based on the interatomic forces at the atomistic scale. However, the representations of a multi-aggregate system with grain boundaries and meso-pores currently exceeds the computational capacity of full atomistic MD models. In this research, we propose a new multiscale methodology to study the system at the atomistic scale and upscale the results to model the formation of clay aggregates. At the meso-scale, microstructure and mechanical properties for a system of clay particles will be calculated and compared with available experiments to validate the performance of the technique in predicting the elastic properties of clay aggregates.

2. Methodology

The proposed method starts with a series of full atomistic molecular simulations of Na-Wyoming montmorillonite clay, $Na_{0.75}\ nH_2$O$[Si_{7.75}Al_{0.25}][Al_{3.5}Mg_{0.5}]O_{20}(OH)_4$, in two basic configurations: edge-to-edge and face-to-face (Figure 1).

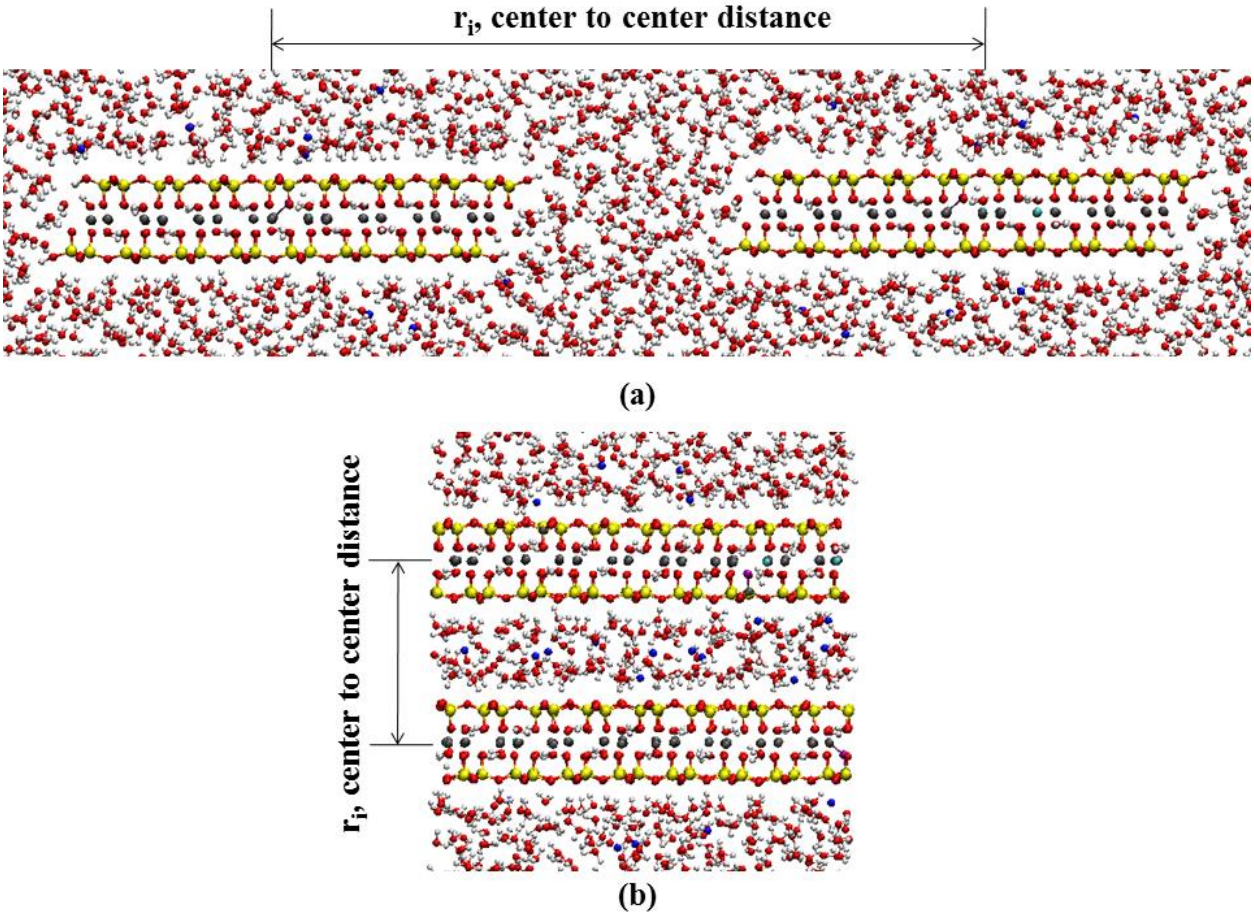

Fig. 1. Part of the typical simulation setup for studying two base interactions : (a) edge-to-edge. (b) face-to-face. (Reproduced with permission from [9]. Copyright 2014, AIP Publishing LLC.)

The center to center distance between clay platelets in each MD simulation is changed in increments of 0.25 Å. All the simulations were performed at pressure of 1 atm and temperature of 300 K. The equations of motions were integrated with an integration time step of 1 fs (femto second). A cut off radius of 8.5 Å was used for short range interactions. Clay platelets were rigid at each specific separation distance. Based on the convergence of the results, each simulation was equilibrated for 0.5 ns (nano second) and results averaged over the following 2.5 ns and 3 ns for edge-to-edge and face-to-face interactions. Each clay platelet consists of sixteen unit cell (4×4 array of clay unit cell) with plan dimensions (X-Y) of ~20.87 Å× ~36.30 Å. Isomorphous substitution of Si^{4+} with Al^{3+} in the tetrahedral layer and Al^{3+} with Mg^{2+} in the octahedral layer were carried out randomly and system neutralized by adding Na atoms. Similar substitution strategy was used previously for layered materials [10, 11]. Periodic boundary conditions were applied to all systems. The trajectory of MD is perturbed to adjacent distances to calculate changes in the Gibbs free energy (ΔG) as a function of the center to center distance using a simple overlap sampling (SOS) technique [12, 13]:

$$\Delta G(r_i \rightarrow r_{i\pm1}) = -\frac{1}{\beta}\ln\left[\frac{\langle exp(-\beta\Delta U/2)\rangle_i}{\langle exp(\beta\Delta U/2)\rangle_{i\pm1}}\right] \quad (1)$$

$\Delta U = U(r_{i\pm1}) - U(r_i)$ and $\beta = (k_B\ T)^{-1}$ where *T* is the temperature, k_B is Boltzmann's constant and U denotes the potential energy of the system. The brackets denote canonical ensemble average over the trajectory and subscript i indicates that the average is taken in the reference state. The change in free energy for edge-to-edge interaction is normalized over the width of the clay platelet to provide the free energy per length (Figure 2(a)) which is then scaled for different platelet sizes with diameter, D. Full atomistic MD simulations were carried out by using the GROMACS [14] simulation package. The atomic structures were visualized using VMD [15] molecular graphic software. The analyses are carried out using the CLAYFF force field [16].

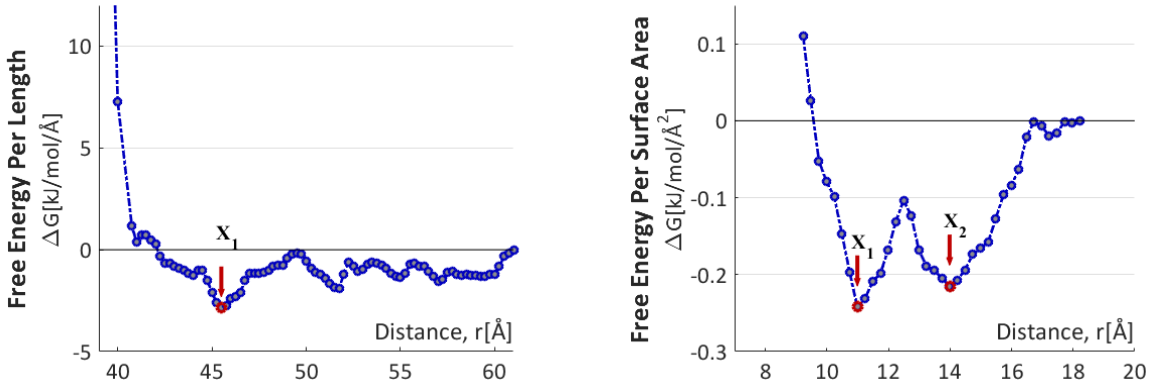

(a) (b)

Fig. 2. (a) Free energy per length for edge-to-edge interaction, There is one main minimum (X_1). (b) Free energy per surface area for face-to-face interaction,there are two comparable minima (X_1 and X_2). (Reproduced with permission from [9]. Copyright 2014, AIP Publishing LLC.)

Figure 2a shows one main minimum for the edge-to-edge interaction at separation distance X_1. The depth and location of this minimum is used in the upscaling procedure. For face-to-face interaction, free energy is presented per surface area by dividing results to the surface of the clay (Figure 2(b)) which is scaled for different platelet sizes using the surface area of the platelet. There are two comparable minima for the face-to-face interaction shown by X_1 and X_2 in Figure 2b corresponding to formation of one and two layers of water molecules between the clay platelets. The current paper uses the first minimum to study clay aggregation. Ebrahimi et al. [9] have shown that this choice of calibration has only a small effect on subsequent simulation of clay aggregate geometry and elastic properties.

At the meso-scale each clay layer is represented by an ellipsoidal shaped particle (Figure 3) (without detailed atomistic structure) and their interaction will be modeled using the Gay-Berne (GB) potential [17].

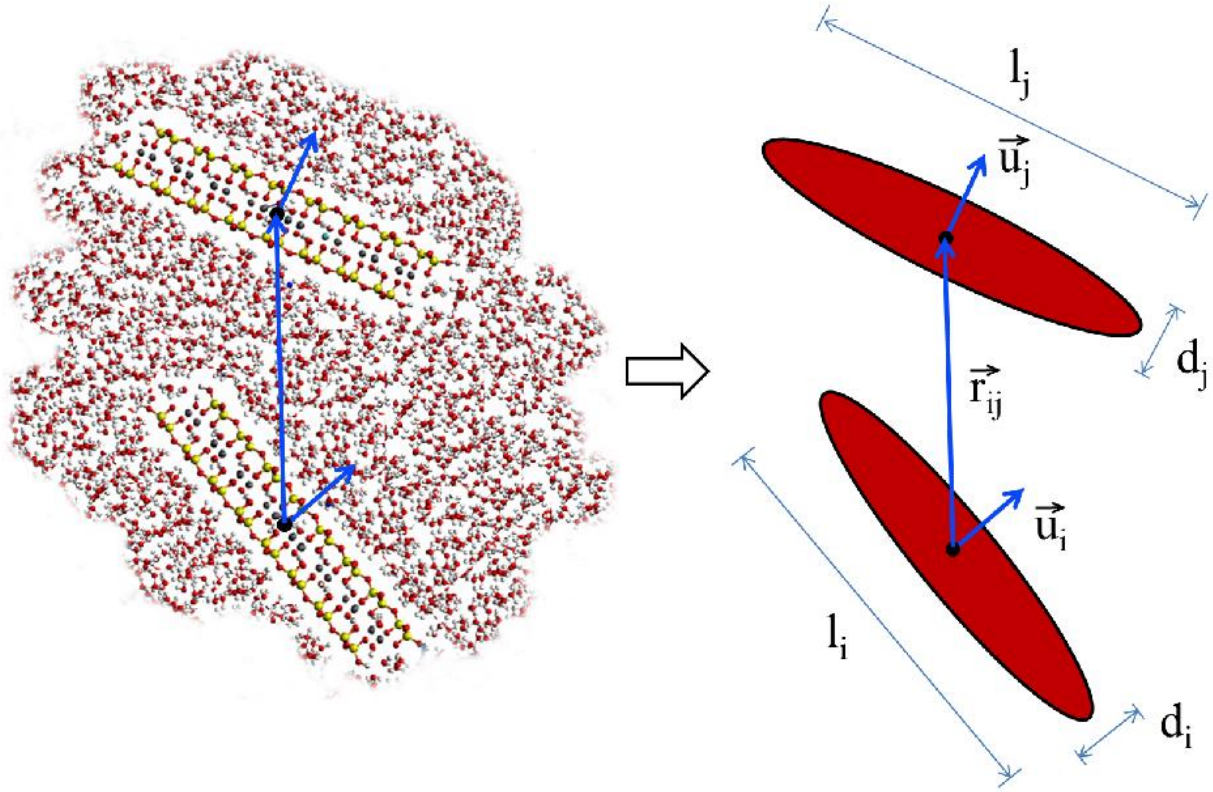

Fig. 3. Approximating each platelet of clay with a new effective ellipsoidal (oblate) particle using the Gay-Berne (GB).

The screening effect of water molecules and ions on the interaction between clay platelets is captured by the calculated free energy. As a result it is possible to reduce the computational cost of modeling assemblies of clay platelets to study the formation of clay aggregates. The GB potential is an anisotropic form of the Lennard-Jones potential. The location and depth of the potential well changes based on the center to center distance between platelets and their relative orientation. By calibrating GB (which needs five parameters for interaction of identical ellipsoidal particles) for edge-to-edge and face-to-face interactions, we can model interactions among system of clay platelets with arbitrary orientations.

Figure 4(a) and (b) show examples of GB potential calibrated for platelets with D=100 Å and D=1000 Å (fitted to X_1 Figure 2(a) and (b)). Meso-scale simulations are performed for three platelet sizes: D=100, 500 and 1000 Å under different confining pressures: P=1, 10, 50, 300 and 800 atm.

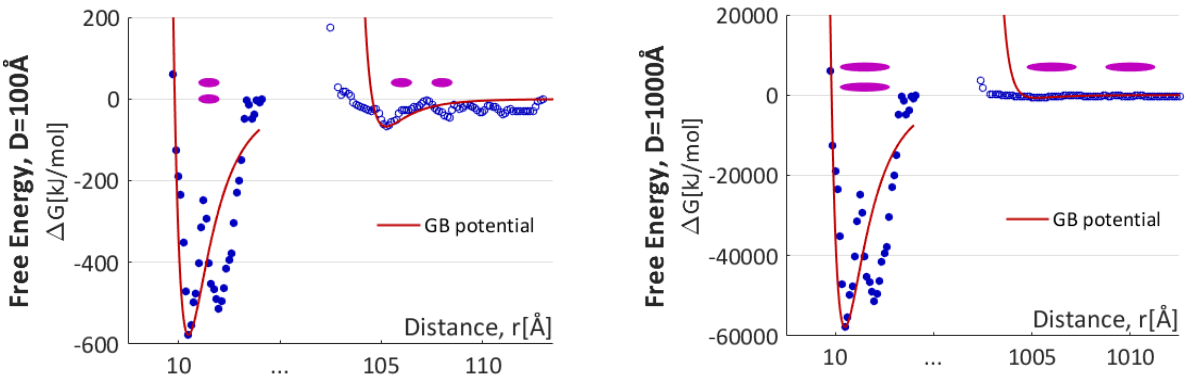

(a) (b)

Fig. 4. Two examples of fitting Gay-Berne (GB) potential to edge-to-edge and face-to-face interaction for clay platelet with different diameters: (a) D=100 Å. (b) D=1000 Å. (Reproduced with permission from [9]. Copyright 2014, AIP Publishing LLC.)

The details of the procedure are explained in [9]. In order to test the performance of the GB potential, free energy of the edge-to-face interaction of platelets was calculated (Figure 5).

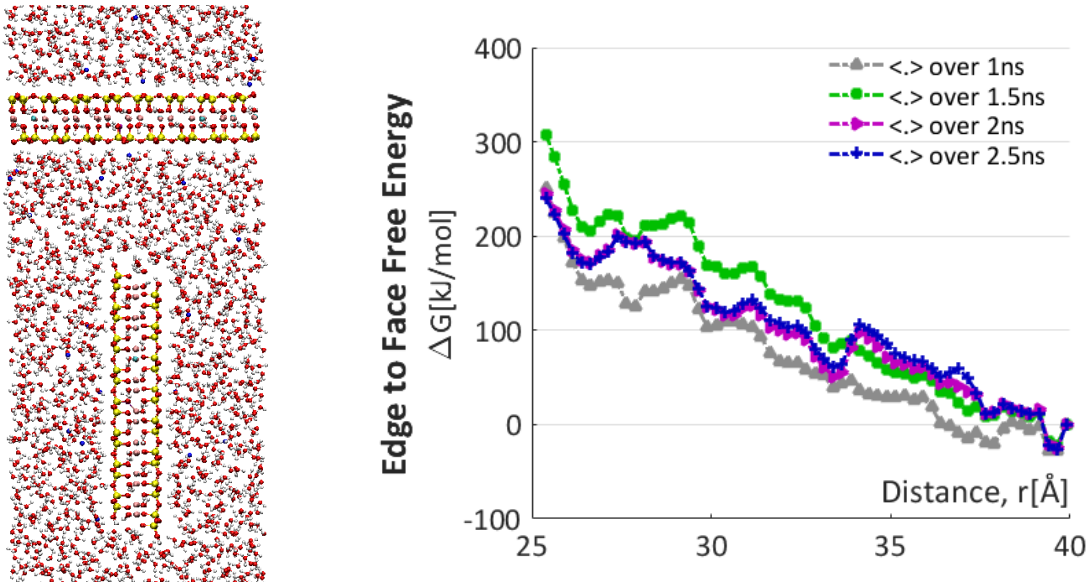

(a) (b)

Fig. 5. (a) Typical simulation setup for studying edge-to-face interaction of clay platelets (b) The calculated potential of mean force shows no attraction for edge-to-face interaction.

Converged results in Figure 5(b) (after averaging over 2.5 ns) show no attraction for edge-to-face interaction. The small attraction close to 40 Å is a boundary artifact. It has been shown that structure and dynamics of water molecules on the clay surface are only affected over two to three molecular layers from the surface[18]. In our face-to-face or edge-to-edge interactions, minima of the potential occurred within the three layers from the surface or edge of the clay platelets. In particular, for the face-to-face interaction which is the strongest interaction due to the surface of the platelets, our results showed that three layers of water completely shields one layer from another. In the current edge-to-face simulations which is the weakest interaction, at ~ 40 Å the thickness of water phase between edge and face of the clay platelet is ~ 18 Å corresponding to about six molecular water layers (diameter of a water molecule ~ 3 Å). As a result, the interaction of two clay platelets is efficiently shielded to have no attraction between the face and edge of the platelet. Prediction of the GB potential for the depth of energy wells are summarized in Table 1. By increasing diameter of the platelet, potential wells become deeper and the difference between face-to-face interaction and edge-to-edge or edge-to-face interactions increases. Fitted GB potentials show negligible attraction for the edge-to-face interaction (less than 5% of the face-to-face interaction) which decreases as platelet diameter increases.

Table 1. Depth of potential wells for face-to-face; edge-to-edge and edge-to-face interactions calculated using GB potential for systems with D = 100; 500; and 1000 Å platelets.

D [Å]	100		500		1000	
	KJ/mol	%	KJ/mol	%	KJ/mol	%
Face-to-face	-578	**100**	-14452	**100**	-57808	**100**
Edge-to-edge	-68	**11.7**	-338	**2.3**	-675	**1.2**
Edge-to-face	-28	**4.8**	-39	**0.3**	-42	**0.07**

3. Results and discussion

Systems of mono-disperse clay platelets were studied under different confining pressures. For each platelet size and confining pressure we simulated ten different samples each containing 1000 platelets with initial random orientations. The average properties of the final states are reported. Each simulation continues until sample compresses to its final fully jammed state. Figure 6 shows percentage of kinetic energy to total energy for typical samples. As platelet size increases from 100 Å to 1000 Å, Ke/Te decreases from 0.25% to 0.0026%. In other words,

temperature becomes irrelevant which is an indication of the jamming state. Transition to the jammed state can be identified by sudden removal of the scatter in the Ke/Te function.

In this section we summarize how the packing structure and elastic properties of clay aggregates varies with the size/diameter of the platelets and the externally applied confining pressure.

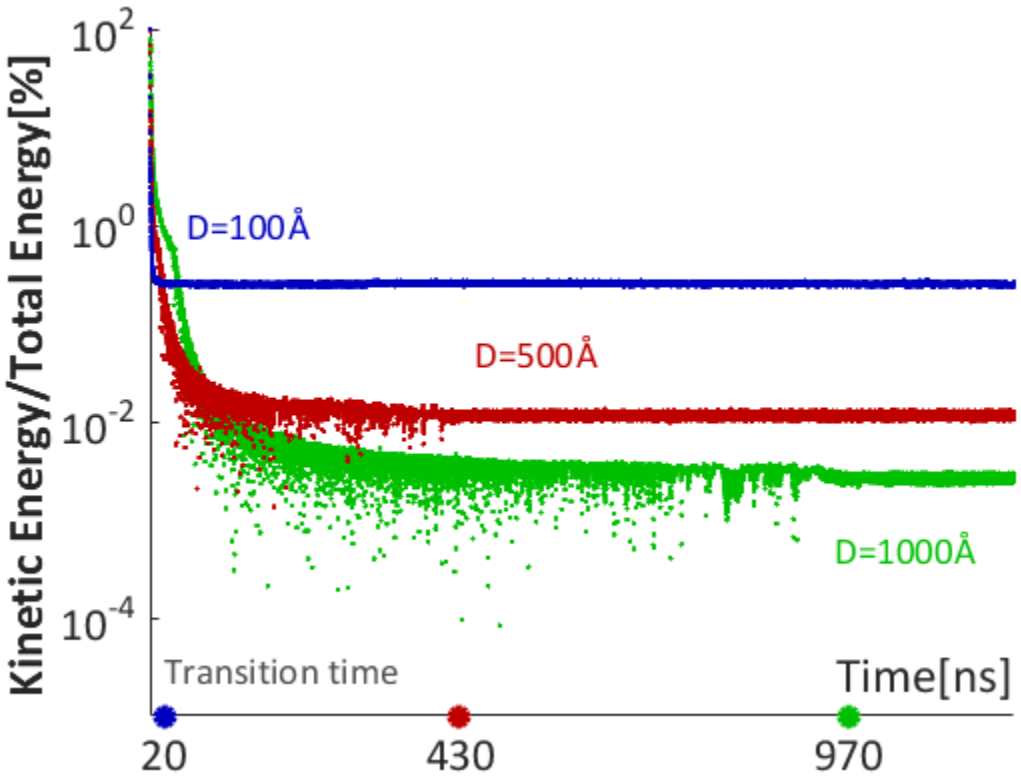

Fig. 6. Sudden removal of scatter in kinetic energy over total energy (Ke/Te) is an indication of final (jamming) state of the system which occurs around 20 ns, 430 ns and 970 ns for 100 Å, 500 Å and 1000 Å platelets, respectively. (Reproduced with permission from [9]. Copyright 2014, AIP Publishing LLC.)

3.1. Microstructure

Typical final states of the particle assemblies are shown Figure 7. We used QMGA package [19] for graphical visualization of the system.

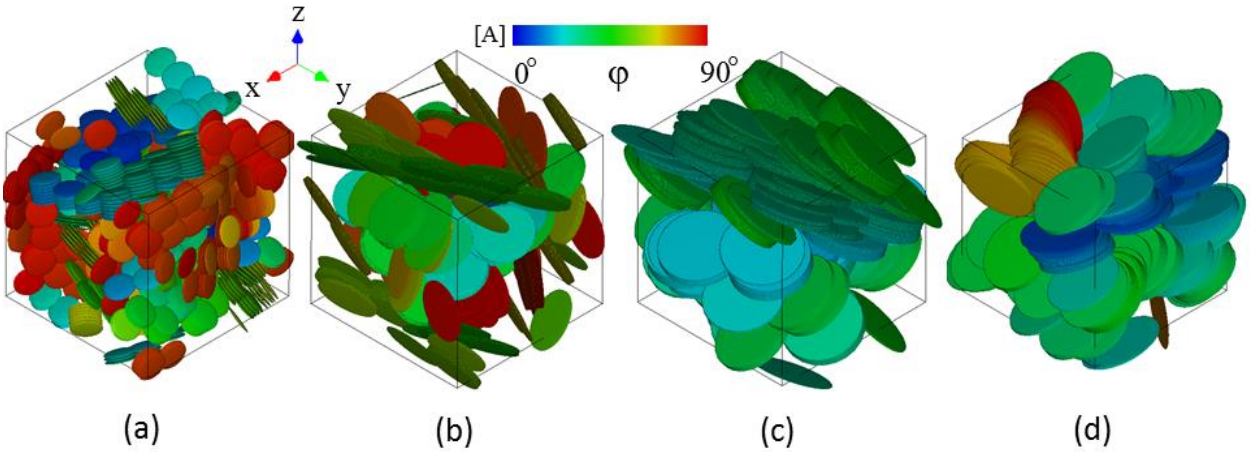

Fig. 7. Examples of the final configuration of the system of particles with diameter, D at pressure, P. (a) D=100 Å, P=1 atm (b) D=1000 Å, P=10 atm (c) D=1000 Å, P=300 atm (d) D=1000 Å, P=800 atm. In (c) and (d) platelets start to slide against each other. The particles orientations are color coded according to the φ angle, orientation of their normal vector with respect to the Z axis (colorbar A). (Reproduced with permission from [9]. Copyright 2014, AIP Publishing LLC.)

The systems of particles are color coded based on the orientation of each platelet with respect to the Z axis. By increasing platelet size (Figure 7(a) vs Figure 7(b)) or increasing pressure (Figure 7(b) vs Figure 7(c)) spectrum of colors decreases which is an indication of more ordered systems. The degree of orientation of particles can be measured using a scalar order parameter, S [20]:

$$S = \left\langle \frac{3\cos^2\theta - 1}{2} \right\rangle \quad (2)$$

where θ is the angle of normal vector of a platelet ($\mathbf{u}$) with director of the system ($\mathbf{n}$). The brackets denote average over all the particles. The director vector of a system of particles, ($\mathbf{n}$), is a measure of the average orientation of the particles in the system. Director is the eigenvector corresponding to largest absolute eigenvalue of the order tensor, q_{ij} :

$$q_{ij} = \frac{1}{N}\sum_{m=1}^{N}\left(u_i u_j - \frac{1}{3}\delta_{ij}\right) \quad (3)$$

where N is the number of particles and δ_{ij} is the Kronecker delta function. For a completely isotropic and randomly oriented system S=0, while perfectly aligned systems have S=1. Figure 8 shows two criteria used for the analysis of aggregate size following [21].

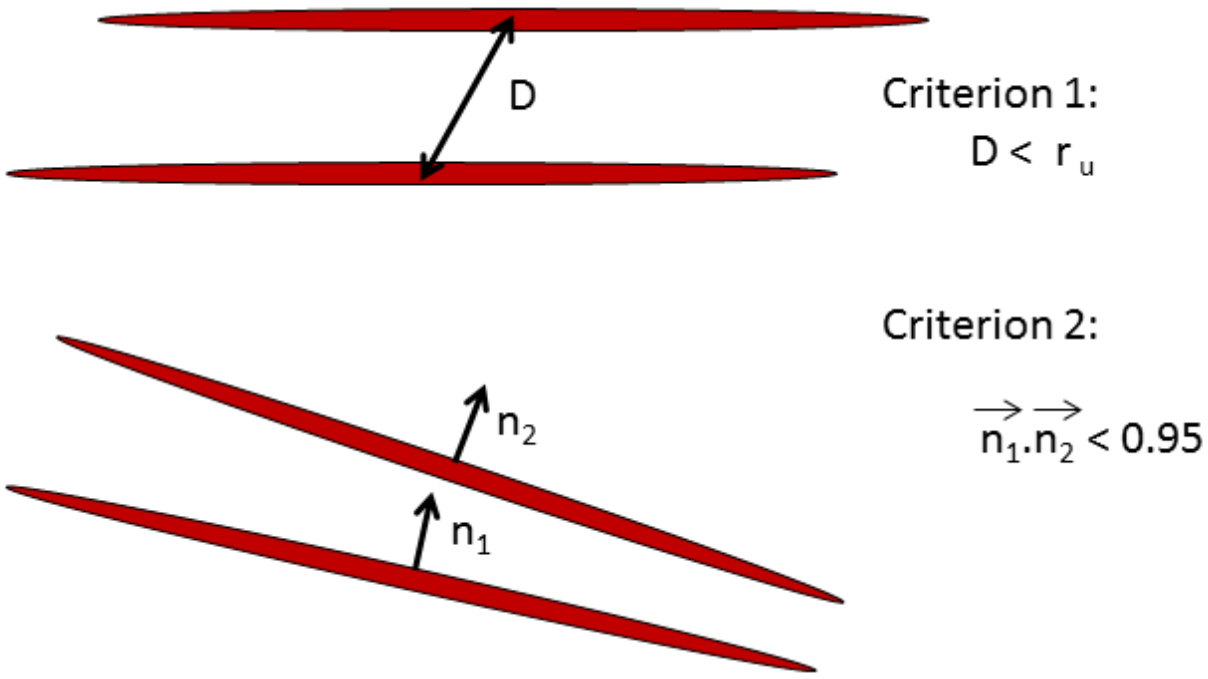

Fig. 8. Two criteria used for the analysis of secondary structures (Aggregates). Both distance (first criterion) and orientation (second criterion) should be satisfied in order to assign two platelets to one aggregate. (Reproduced with permission from [9]. Copyright 2014, AIP Publishing LLC.)

The distance between platelets should be less than an upper limit, r_u (first criterion) and they should stack on top of each other (second criterion). The current analysis assumes that r_u is 25% larger than the first face-to-face equilibrium distance (X_1 in Figure 2(b)) to allow for offsetting of platelets, $r_u = 13.75$ Å. Both criteria should be met in order to assign two platelets to an aggregate.

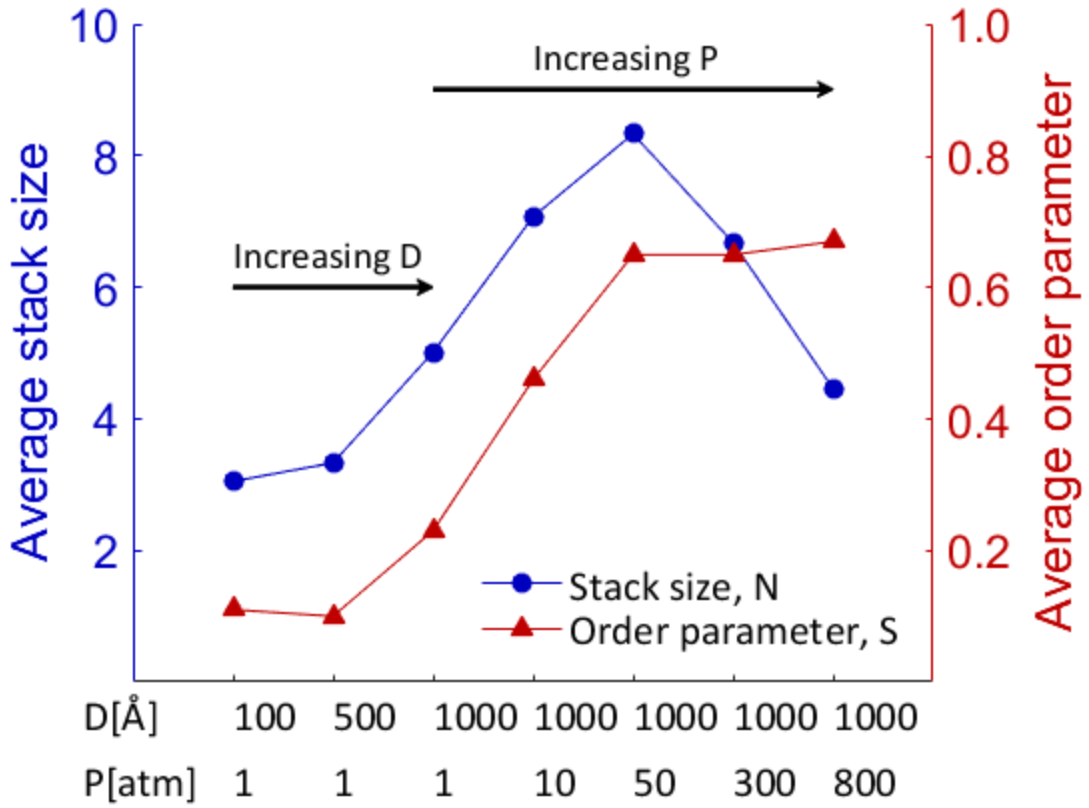

Fig. 9. Circles: By increasing size of the clay platelet from D=100 Å to 1000 Å (P=1 atm), average stack size per aggregate increases from 3 to 5. For D=1000 Å, by increasing pressure from 1 atm to 10 atm and 50 atm average stack size increases from 5 to 8. Further increase of pressure to 300 atm and 800 atm results in decrease in the average stack size. Triangles: Change of the average order parameter is consistent with the change in average stack size. System becomes more ordered as pressure increases up to 50 atm. Further increase of pressure has no effect on the orientation of particles (S~0.65).

Figure 9 shows results of the geometrical analysis of the aggregates. By increasing platelet size from D=100 Å to D=1000 Å, the average number of platelets per aggregate increases from 3 to 5 since larger platelets can interact with larger number of neighboring platelets as interactions scale with the surface area. Increase of pressure from 1 to 10 to 50 atm results in larger aggregates (up to 8 platelets per aggregate). The order parameter of the system follows the same trend. By increasing platelet size, the system becomes more ordered (i.e., S value increases). In other words, smaller platelets have more freedom to move around and as a result produce a more isotropic particle assembly with random orientation in agreement with experiments [22]. When the pressure is increased up to 50 atm the platelets develop a more anisotropic structure (order parameter increases to S~0.65). This point is the maximum ordered state for the system. Further increase of pressure (to 300 and 800 atm) has no effect on the orientation of particles (S remains constant) and the platelets start to slide against each other (more than r_u in Figure 8) as seen in Figures 7(c) and (d). As a result, the mean aggregate size decreases to $\sim$ 4. Using transmission electron microscopy, scanning electron microscopy,

small angle X-ray scattering and X-ray diffraction experiments on different types of Na-smectites, the average number of platelets per aggregate has been measured between 3 to 10 in agreement with current numerical simulations [22–26].

3.2. Mechanical properties

Mechanical properties of the system are calculated by computing the stress-strain and reporting elastic stiffness values in the initial small strain regime (see [27]). For the system of ellipsoidal particles under confining pressure the elastic properties can be approximated using cubic symmetry assumption with three parameters:
$\overline{C}_{11} = 1/3(C_{11} + C_{22} + C_{33})$,$\overline{C}_{44} = 1/3(C_{44} + C_{55} + C_{66})$,
$\overline{C}_{12} = 1/3(C_{12} + C_{13} + C_{23})$
(See [9] for more detail). The results are summarized in Table 2. By increasing size of the platelet normal stiffness, $\overline{C}_{11}$, increases (from 0.51 GPa to 0.98 GPa) while the shear stiffness, $\overline{C}_{44}$, and the component related to the Poisson's effect, $\overline{C}_{12}$, show negligible change. Ebrahimi et al. [9] show that when the GB potential is calibrated using the second energy well (for face-face interactions) there is a 25% reduction in stiffness properties, compared to values reported in Table 2. All elastic constants increase with increasing confining pressure as expected.

Table 2. Cubic averaged elastic properties (in GPa) of the elasticity tensor for different platelet diameter, D and confining pressure, P. (Reproduced with permission from [9]. Copyright 2014, AIP Publishing LLC.)

D [Å]	500	1000	1000	1000	1000	1000
P [atm]	1	1	10	50	300	800
$\overline{C}_{11}$	0.51	0.98	4.07	6.42	14.17	29.16
$\overline{C}_{12}$	0.13	0.14	0.53	1.24	4.12	8.80
$\overline{C}_{44}$	0.10	0.08	0.44	0.66	1.91	4.68

In order to validate mechanical properties we calculated indentation modulus from elastic constants (C_{ij}) using the derivation by Delafargue and Ulm [28] for an orthotropic solid and compared the mesoscale model predictions with experimental indentation modulus on shale and clay samples reported by Bobko and Ulm [29]. The current simulations do not represent the formation conditions of natural shale specimens but provide a first order comparison based on micro-porosity. The largest dimension of clay platelet used in simulation was 1000 Å which is at least ten times smaller than size of nanoplatelets found in shale. Moreover, platelets of clay are assumed to be rigid. We believe that the microstructure from the current mesoscale simulations is similar to randomly oriented clay platelets which form phyllosilicate framework

(PF) pores in shale at submicron length scale[30]. The mean indentation modulus shows good agreement with measured values and follows the same trend with packing density as shown in Figure 10.

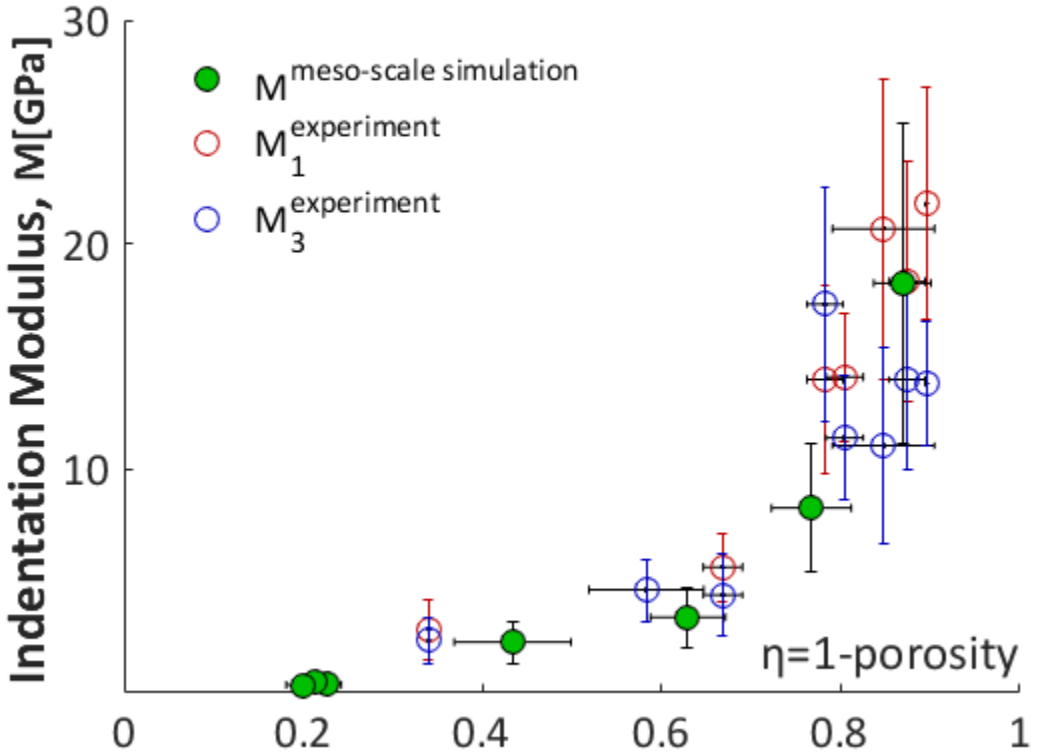

Fig. 10. Comparison of indentation modulus versus clay packing density, η between simulation results (for different platelet diameters and different pressures) and experimental data taken from Bobko and Ulm [29]. Subscripts 1 and 3 stand for indentation parallel and normal to the bedding plane. (Reproduced with permission from [9]. Copyright 2014, AIP Publishing LLC.)

4. Conclusions

We propose a new methodology to study aggregation of clay particles at the meso-scale based on the atomistic interaction between two clay platelets in an aqueous environment. Full atomistic simulation of the clay (Na-Wyoming montmorillonite)-water system for edge-to-edge and face-to-face interaction of clay platelets were used to calculate changes in free energy as a function of the separation distance using perturbation theory. At the meso-scale clay platelets were approximated by ellipsoidal particles and their interaction for different orientations were defined using Gay-Berne potential calibrated for edge-to-edge and face-to-face interactions from the atomistic scale. Results of the simulations show an increase in the average aggregate size by increasing platelet diameter. An increase in the confining pressure creates a more

ordered system and average aggregate size increases until reaching to a maximum ordered state. Further increase of pressure results in decrease in average aggregate size since orientation of platelets remains constant and they start to slide against each other. The computed mean stack size (3-8) for Na-smectite is in good agreement with experiments (3-10). Moreover, our mesoscale model is also able to match quite closely the measured elastic indentation modulus for shale and clay specimens over a wide range of packing density. The current analyses are limited to a single species of smectite (Na-Wyoming montmorillonite) with cation exchange capacity, CEC = 102 meq/100g and mono-disperse assemblies of platelets. The method can be used to study the effect of amount and type of isomorphous substitution on the microstructure and mechanical properties of clay aggregates. The heterogeneity of the platelet sizes at the meso-scale can change the distribution of aggregate sizes. The research can be extended to study effects of polydisperse assemblies of clay platelets.

References

1. Boivin, P., Garnier, P., Tessier, D.: Relationship between clay content, clay type, and shrinkage properties of soil samples. Soil Sci. Soc. Am. J. 68, 1145–1153 (2004).
2. Żbik, M.S., Frost, R.L., Song, Y.-F., Chen, Y.-M., Chen, J.-H.: Transmission x-ray microscopy reveals the clay aggregate discrete structure in aqueous environment. J. Colloid Interface Sci. 319, 457–461 (2008).
3. Wagner, S., Cattle, S.R., Scholten, T.: Soil-aggregate formation as influenced by clay content and organic-matter amendment. J. Plant Nutr. Soil Sci. 170, 173–180 (2007).
4. Verwey, E.J.W., Overbeek, J.T.G., Overbeek, J.T.G.: Theory of the stability of lyophobic colloids. Courier Corporation (1999).
5. Derjaguin, B.V., Landau, L.: The theory of stability of highly charged lyophobic sols and coalescence of highly charged particles in electrolyte solutions. Acta Physicochim URSS. 14, 633–52 (1941).
6. Israelachvili, J.N., Pashley, R.M.: Molecular layering of water at surfaces and origin of repulsive hydration forces. Nature. 306, 249–250 (1983).
7. Pashley, R.M., Israelachvili, J.N.: Molecular layering of water in thin films between mica surfaces and its relation to hydration forces. J. Colloid Interface Sci. 101, 511–523 (1984).
8. Ebrahimi, D., Pellenq, R.J.-M., Whittle, A.J.: Nanoscale elastic properties of montmorillonite upon water adsorption. Langmuir. 28, 16855–16863 (2012).
9. Ebrahimi, D., Whittle, A.J., Pellenq, R.J.-M.: Mesoscale properties of clay aggregates from potential of mean force representation of interactions between nanoplatelets. J. Chem. Phys. 140, 154309 (2014).

10. Abdolhosseini Qomi, M.J., Ulm, F.-J., Pellenq, R.J.-M.: Evidence on the Dual Nature of Aluminum in the Calcium-Silicate-Hydrates Based on Atomistic Simulations. J. Am. Ceram. Soc. 95, 1128–1137 (2012).

11. Abdolhosseini Qomi, M.J., Krakowiak, K.J., Bauchy, M., Stewart, K.L., Shahsavari, R., Jagannathan, D., Brommer, D.B., Baronnet, A., Buehler, M.J., Yip, S., Ulm, F.-J., Van Vliet, K.J., Pellenq, R..-. M.: Combinatorial molecular optimization of cement hydrates. Nat Commun. 5, (2014).

12. Chipot, C., Pohorille, A.: Free energy calculations. Springer (2007).

13. Lee, C.Y., Scott, H.L.: The surface tension of water: A Monte Carlo calculation using an umbrella sampling algorithm. J. Chem. Phys. 73, 4591–4596 (1980).

14. Hess, B., Kutzner, C., Van Der Spoel, D., Lindahl, E.: GROMACS 4: algorithms for highly efficient, load-balanced, and scalable molecular simulation. J. Chem. Theory Comput. 4, 435–447 (2008).

15. Humphrey, W., Dalke, A., Schulten, K.: VMD: visual molecular dynamics. J. Mol. Graph. 14, 33–38 (1996).

16. Cygan, R.T., Liang, J.-J., Kalinichev, A.G.: Molecular models of hydroxide, oxyhydroxide, and clay phases and the development of a general force field. J. Phys. Chem. B. 108, 1255–1266 (2004).

17. Gay, J.G., Berne, B.J.: Modification of the overlap potential to mimic a linear site–site potential. J. Chem. Phys. 74, 3316–3319 (1981).

18. Marry, V., Rotenberg, B., Turq, P.: Structure and dynamics of water at a clay surface from molecular dynamics simulation. Phys. Chem. Chem. Phys. 10, 4802–4813 (2008).

19. Gabriel, A.T., Meyer, T., Germano, G.: Molecular graphics of convex body fluids. J. Chem. Theory Comput. 4, 468–476 (2008).

20. Prost, J.: The physics of liquid crystals. Oxford university press (1995).

21. Chen, C.-T., Ball, V., de Almeida Gracio, J.J., Singh, M.K., Toniazzo, V., Ruch, D., Buehler, M.J.: Self-assembly of tetramers of 5, 6-dihydroxyindole explains the primary physical properties of eumelanin: Experiment, simulation, and design. ACS Nano. 7, 1524–1532 (2013).

22. Hetzel, F., Tessier, D., Jaunet, A.-M., Doner, H.: The Microstructure of Three Na^+ Smecites: The Importance of Particle Geometry on Dehydration and Rehydration. Clays Clay Miner. 42, 242–242 (1994).

23. Tessier, D., Pedro, G.: Electron microscopy study of Na smectite fabric—role of layer charge, salt concentration and suction parameters. In: Proceedings of the International Clay Conference, Bologna and Pavia, Italy. pp. 6–12 (1981).

24. Pons, C.H., Tessier, D., Rhaiem, H.B., Tchoubar, D., Van Olphen, H., Veniale, F.: A comparison between X-ray studies and electron microscopy observations of smectite fabric. In: International Clay Conference. pp. 177–185. Elsevier (1981).

25. Rhaiem, B.: Factors affecting the microstructure of smectites–role of cation and history of applied stresses. In: Proceedings of the International Clay Conference. pp. 292–7 (1985).

26. Mystkowski, K., Środoń, J., Elsass, F.: Mean thickness and thickness distribution of smectite crystallites. Clay Miner. 35, 545–557 (2000).

27. Aghaei, A., Qomi, M.A., Kazemi, M.T., Khoei, A.R.: Stability and size-dependency of Cauchy–Born hypothesis in three-dimensional applications. Int. J. Solids Struct. 46, 1925–1936 (2009).

28. Delafargue, A., Ulm, F.-J.: Explicit approximations of the indentation modulus of elastically orthotropic solids for conical indenters. Int. J. Solids Struct. 41, 7351–7360 (2004).

29. Bobko, C., Ulm, F.-J.: The nano-mechanical morphology of shale. Mech. Mater. 40, 318–337 (2008).

30. Schieber, J., others: Common themes in the formation and preservation of intrinsic porosity in shales and mudstones-illustrated with examples across the Phanerozoic. In: SPE Unconventional Gas Conference. Society of Petroleum Engineers (2010).